

Eddy transport as a key component of the Antarctic overturning circulation

Andrew F. Thompson^{1*}, Karen J. Heywood², Sunke Schmidtko^{2,3} and Andrew L. Stewart^{1,4}

The exchange of water masses across the Antarctic continental shelf break regulates the export of dense shelf waters to depth as well as the transport of warm, mid-depth waters towards ice shelves and glacial grounding lines¹. The penetration of the warmer mid-depth waters past the shelf break has been implicated in the pronounced loss of ice shelf mass over much of west Antarctica^{2–4}. In high-resolution, regional circulation models, the Antarctic shelf break hosts an energetic mesoscale eddy field^{5,6}, but observations that capture this mesoscale variability have been limited. Here we show, using hydrographic data collected from ocean gliders, that eddy-induced transport is a primary contributor to mass and property fluxes across the slope. Measurements along ten cross-shelf hydrographic sections show a complex velocity structure and a stratification consistent with an onshore eddy mass flux. We show that the eddy transport and the surface wind-driven transport make comparable contributions to the total overturning circulation. Eddy-induced transport is concentrated in the warm, intermediate layers away from frictional boundaries. We conclude that understanding mesoscale dynamics will be critical for constraining circumpolar heat fluxes and future rates of retreat of Antarctic ice shelves.

Residual-mean theories, which propose a leading-order balance between wind- and eddy-induced overturning cells, have illuminated the dynamics of material exchange across the Southern Ocean's Antarctic Circumpolar Current⁷ (ACC). The Antarctic margins share similarities with the ACC: the circulation is composed of strong, narrow frontal currents; the flow is unblocked by continental boundaries; and surface forcing is largely due to zonal, down-front winds—easterlies around Antarctica, westerlies over the ACC. Evidence of persistent eddy variability in both idealized and realistic numerical models^{5,6,8–10}, as well as mooring data¹¹, has led to the proposal that wind-driven and eddy overturning cells may be active at the Antarctic margins^{9,10,12}. Observational confirmation requires resolving variability in along-stream velocity and cross-stream buoyancy fields. We present new hydrographic data that achieves this coverage and supports the presence of an eddy overturning at the shelf break.

Three ocean gliders were deployed in the northwestern Weddell Sea between 20 January and 13 March 2012 (Fig. 1a,b). This region is a key gateway for the delivery of Antarctic Bottom Water (AABW) to the Scotia Sea, and eventually to the global circulation¹³. Furthermore, the export of iron-rich shelf waters gives rise to elevated chlorophyll levels in the Scotia Sea^{14,15},

which distinguishes this region from most of the Southern Ocean, where nutrients are replete but chlorophyll levels are low. Therefore, cross-slope exchange processes influence both the global overturning circulation and Southern Ocean biogeochemical and ecosystem dynamics.

Properties of AABW are modified near the Antarctic coast owing to entrainment or mixing with modified Circumpolar Deep Water¹⁶ (MCDW). These interactions are enhanced at the shelf break, where MCDW penetrates onshore, establishing strong lateral water-mass gradients (Fig. 1c; glider section A). MCDW intrudes on the shelf, separating cold Winter Water above and relatively fresh Weddell Sea Deep Water below; other glider sections are similar. The injection of warm MCDW onto the shelf occurs through intermittent pulses, consistent with an energetic mesoscale field. Temperature/salinity diagrams (Fig. 1d,e) indicate that the space enclosed by the three water-mass endmembers is populated by many observations, indicative of strong mixing both along and potentially across density surfaces. Lateral stirring throughout the water column will expose a broad range of density classes to mixing, which will in turn influence the closure of the meridional overturning circulation's lower cell at the southern boundary^{17,18}.

The high-resolution glider sections provide a striking view of the cross-slope structure of the Antarctic Slope Front (ASF) system¹⁹. Rather than a single ASF shelf-break current¹, the glider sections reveal a more complex picture (Supplementary Fig. 1). A narrow, bottom-intensified current is nearly always found at, or slightly offshore of the shelf break. Yet, as many as three distinct velocity cores may span a distance as short as 50 km. These small-scale fronts have a baroclinic structure and are not simply a signature of a variable barotropic transport. The front separation remains larger than the first baroclinic Rossby deformation radius λ , which we estimate as $\lambda = NH/f \approx 5\text{--}10$ km, where N is the buoyancy frequency, H is the water column depth and f is the Coriolis frequency (see Methods for values). In a turbulent flow, potential vorticity (PV) gradients, due to a change in water column depth for instance, can give rise to banded flows, or jets. A standard scaling for the separation of these jets depends on an eddy velocity U_e and the background PV gradient, in this case a topographic beta β_T , yielding the Rhines scale $\ell_R \sim \sqrt{U_e/\beta_T}$. Using the root mean square value of velocities over the continental slope, $U_e \approx 0.1$ m s⁻¹, and the scaling $\beta_T \sim fH^{-1}\partial H/\partial y$, we arrive at $\ell_R \approx 20$ km. This is consistent with the observed spacing of the velocity cores, and further evidence of an active mesoscale eddy field.

¹Environmental Science and Engineering, California Institute of Technology, MC 131-24, 1200 East California Boulevard, Pasadena, California 91125, USA,

²School of Environmental Sciences, University of East Anglia, Norwich Research Park, Norwich NR4 7TJ, UK, ³GEOMAR, Helmholtz Center for Ocean Research, Düsternbrooker Weg 20, D-24105 Kiel, Germany, ⁴Los Angeles Department of Atmospheric and Oceanic Sciences, University of California, Los Angeles, California 90095, USA. *e-mail: andrewt@caltech.edu

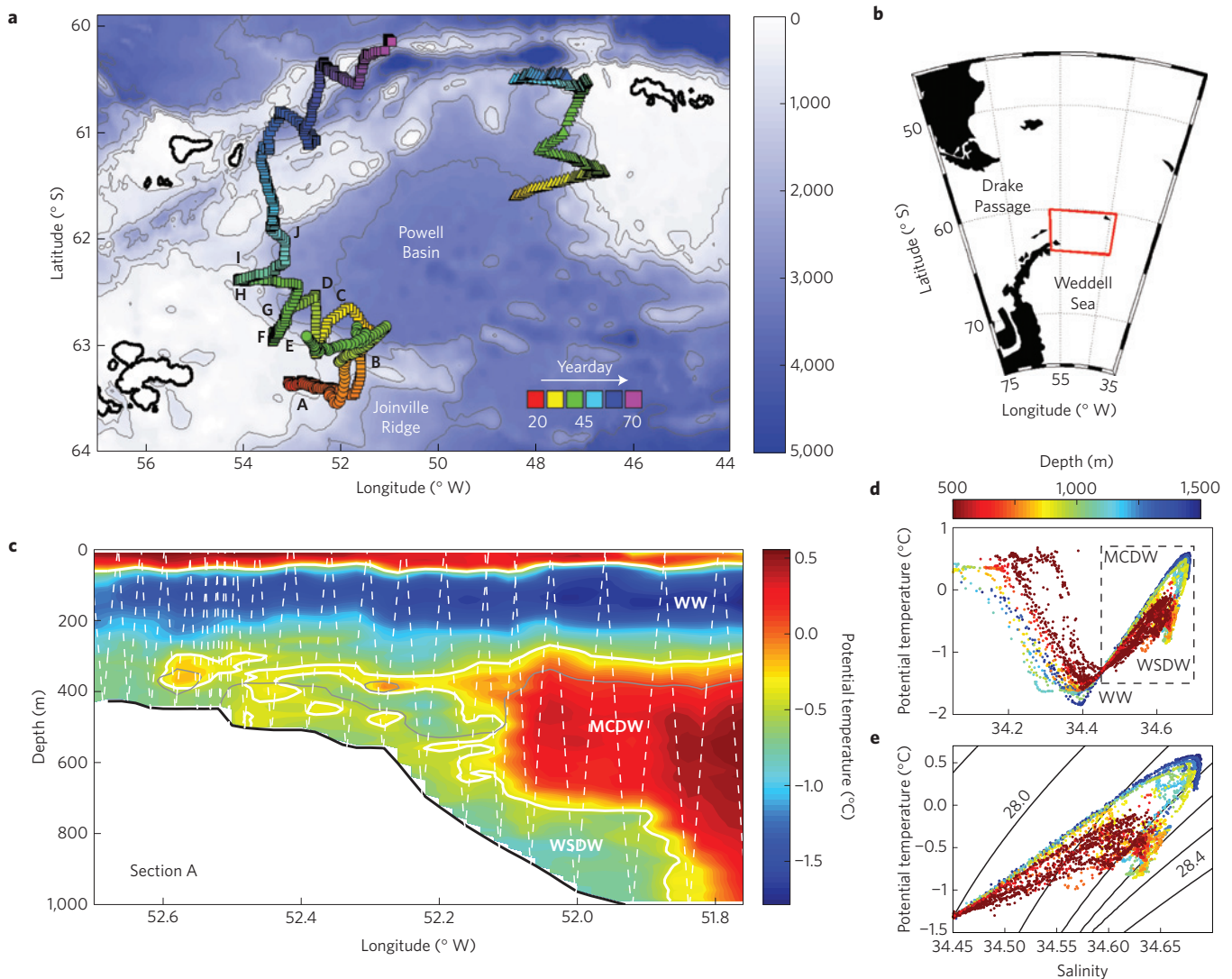


Figure 1 | Overview of the study region. **a**, Map of the northwestern Weddell Sea showing the position of hydrographic profiles from three ocean gliders. The background colour shows depth (m); the symbol colour shows the temporal evolution of the glider positions. **b**, Location of **a**, **c**. Potential temperature along section A; water masses include Winter Water (WW), modified Circumpolar Deep Water (MCDW) and Weddell Sea Deep Water (WSDW). The dashed line shows the position of the glider observations. The grey contour shows the 34.61 isohaline. **d**, Temperature/salinity diagram for section A; colour indicates depth of the water column (m) at the measurement position. **e**, Expanded view of the outlined region in **d**. The contours are isolines of neutral density; contour spacing is 0.1 kg m^{-3} .

We next present maps of PV (defined in Methods, equation (3)) to diagnose eddy mass transport. PV is a conservative tracer along density surfaces if diabatic processes are small, and mesoscale stirring is assumed to relax PV gradients. Similar to the ACC (ref. 7) or the mid-latitude atmospheric circulation²⁰, a down-gradient flux of PV by eddies acts to relax density layer thickness gradients. In other words, eddies flux mass down thickness gradients through a residual velocity vector \mathbf{v}_{res} , defined as $\overline{\mathbf{v}'h'}/\bar{h}$, where h is the thickness of a density layer and \mathbf{v} is the horizontal velocity vector; $(\overline{\cdot})$ implies a time and along-stream average and primed quantities are deviations from this mean. Applying a diffusive parameterization gives $\mathbf{v}_{\text{res}}\bar{h} \approx -K\nabla\bar{h}$, where K is an eddy diffusivity⁷. At the Antarctic margins, thickness gradients are largest in the cross-slope direction.

Distributions of PV are similar across the different glider sections (Fig. 2 and Supplementary Fig. 2). PV is enhanced at the shelf break, consistent with the V-shaped structure of the ASF (ref. 1). Over the continental slope, PV anomalies arise owing to the cross-slope advection of density surfaces by Ekman transport

in frictional boundary layers²¹. Mapping the PV distribution into density, as opposed to depth, coordinates reveals substantial along-isopycnal PV (or thickness) gradients, in some cases exceeding an order of magnitude change in PV over 50 km. Density layers shoal moving towards the shelf break, but they also thin. Figure 2c shows the thickness of three density classes, superimposed on the cross-section velocity field. Each layer exhibits a large-scale thinning towards the shelf break. In the lowermost layer, the thickness gradient is enhanced across the width of the bottom-intensified ASF. This is a common feature in the different sections that can arise from the vertical advection of density surfaces where the bottom Ekman transport is convergent (Fig. 3b). This increase in the thickness gradient may balance a suppression of cross-slope transport associated with the ASF. Overall, down-gradient PV fluxes acting on the observed stratification result in an onshore eddy flux of MCDW throughout most of the water column. The meridional transport is a combination of this eddy transport and Ekman transports in top and bottom boundary layers.

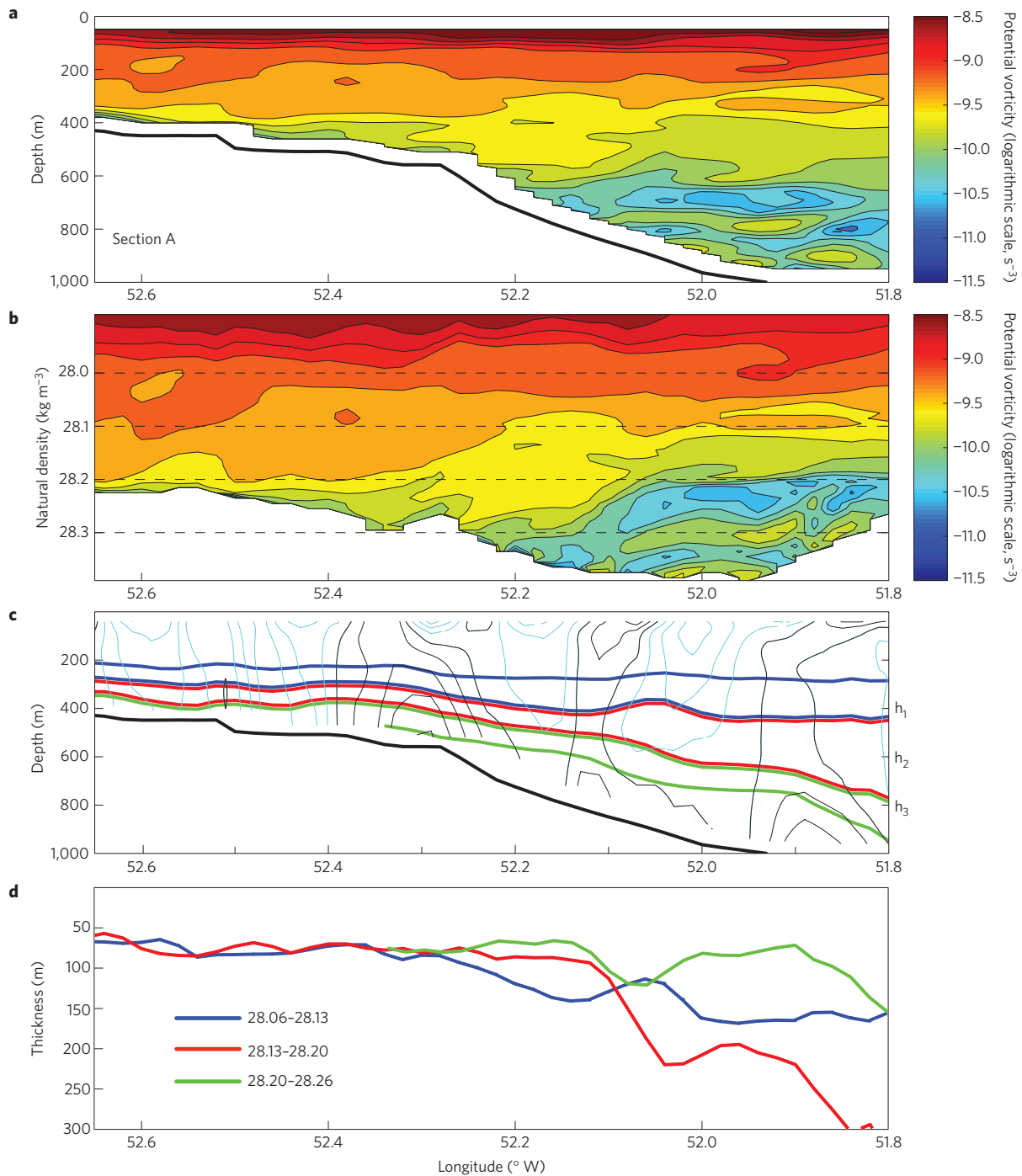


Figure 2 | Cross-slope PV characteristics. **a**, PV (logarithmic axis, for example, $-9=10^{-9} \text{ s}^{-3}$) along section A from Fig. 1a; PV is defined in the Methods. The solid black line indicates the continental shelf/slope. **b**, PV mapped into neutral density coordinates for the same section. **c**, Bold curves show neutral density contours along section A; thin contours are the along-slope geostrophic velocities. Contours are every 4 cm s^{-1} with black (cyan) indicating cyclonic (anticyclonic) flow. **d**, Thickness of the neutral density classes (described in the legend, kg m^{-3}) from **c**.

The relative magnitude of the wind-forced and eddy-induced overturning, ψ_w and ψ_e respectively, can be estimated from a scaling analysis. The surface Ekman transport is given by $\psi_w = -\tau / (\rho_0 f)$, where τ is the along-slope surface wind stress and ρ_0 is a reference density⁷, whereas $\psi_e = v' h' = -K \partial_y \bar{h}_{\text{CDW}}$, where $\partial_y \bar{h}_{\text{CDW}}$ is the cross-slope thickness gradient of the CDW density layer. To estimate K , we apply a well-tested parameterization²²,

$$K = \alpha \frac{M^2}{N} \ell^2 \quad (1)$$

where M^2 and N^2 are lateral and vertical buoyancy gradients respectively, ℓ is the horizontal scale of the baroclinic front and $\alpha = 0.015$. Equation (1) is an accurate scaling in eddy-resolving simulations¹⁰. Applying values calculated from the glider data (provided in Methods) gives

$$K \approx 14 \text{ m}^2 \text{ s}^{-1}, \quad \psi_e \approx -0.14 \text{ m}^2 \text{ s}^{-1}, \quad \psi_w \approx -0.30 \text{ m}^2 \text{ s}^{-1}, \quad \frac{\psi_e}{\psi_w} = 0.47 \quad (2)$$

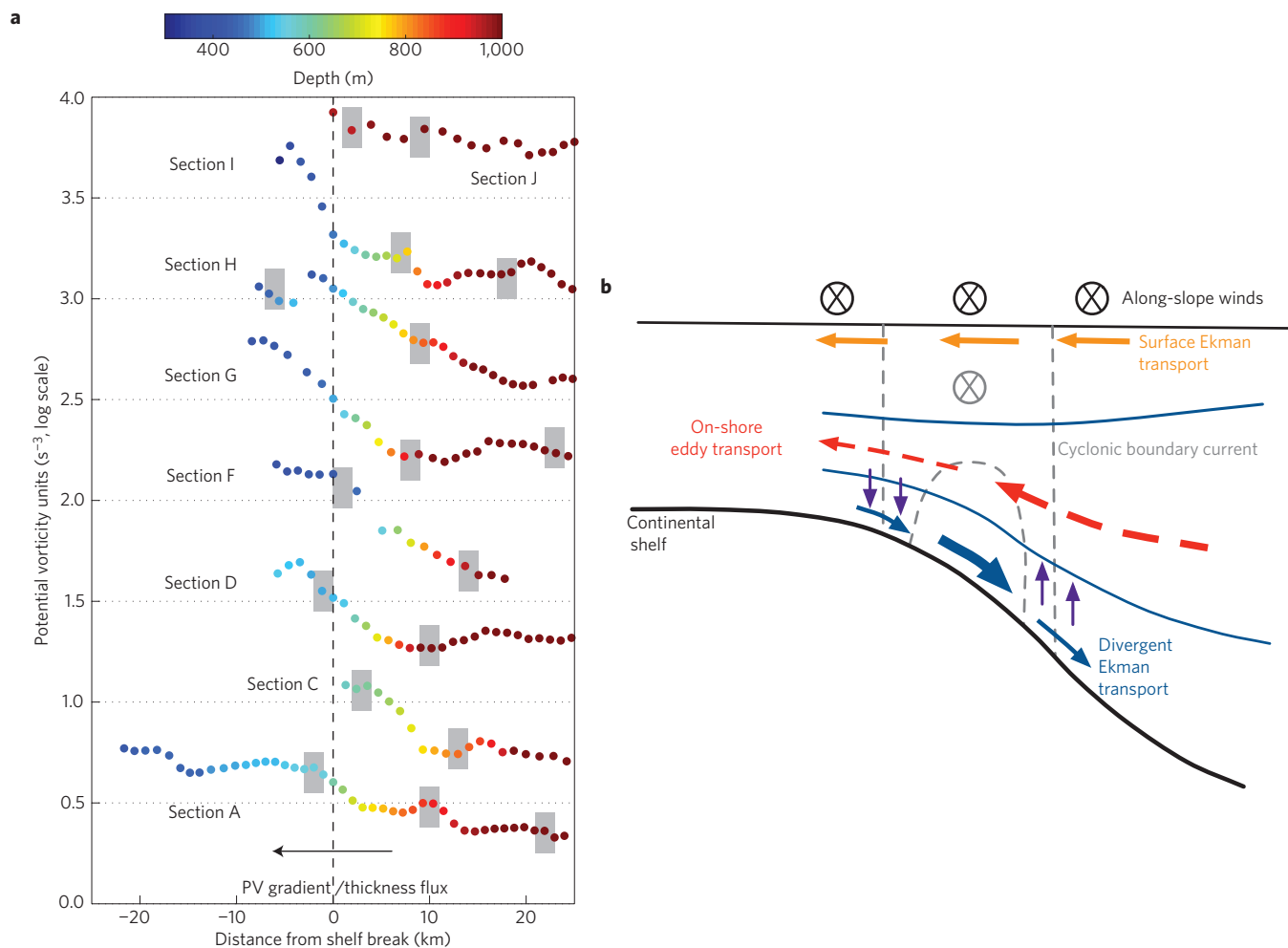


Figure 3 | Summary of cross-slope exchange. **a**, Summary of the PV structure for all sections. The cross-slope position is normalized by distance from the shelf break and sections are offset vertically for clarity. The abscissa is given in logarithmic units of PV. The values plotted are the mean PV over the density class $28.1 < \gamma^n < 28.2$. Colour indicates the water column depth and grey blocks indicate the position of fronts with a bottom velocity greater than 0.15 m s^{-1} . The black arrow indicates the direction of the PV gradient and the subsequent direction of the eddy mass flux. **b** Schematic diagram of key components of the Antarctic marginal meridional overturning. See text for description.

Thus, ψ_e makes a critical contribution to the total overturning, which is the sum of ψ_w and ψ_e , and is balanced by the offshore transport in the bottom boundary layer.

The along-stream-averaged approach suggests that other sections should be statistically similar. A sustained onshore PV gradient is found along all sections crossing the shelf break in the northwestern Weddell Sea (Fig. 3), consistent with an onshore eddy transport at intermediate depths. The grey blocks in Fig. 3a indicate the locations of strong, bottom-intensified velocities. In sections A, C, F, G, H, I and J these frontal positions are associated with local modifications to the PV gradient, which imply a small-scale modification of K across the fronts.

The observed PV gradients confirm the key elements of the Antarctic marginal overturning circulation, summarized in Fig. 3b. Wind stress typically produces an onshore Ekman transport and a sea surface height gradient consistent with a westward geostrophic flow at the shelf break^{1,19}. The continental slope focuses the along-slope flow into narrow frontal currents owing to a preference for flow along contours of f/H (conservation of PV). In regions of dense water export, slope currents are bottom intensified. A frictional down-slope Ekman transport arises that is proportional to the frontal speed above the bottom Ekman layer²³. Lateral shear in

the frontal currents produces regions of bottom Ekman convergence (offshore) and divergence (onshore). In the interior, the flow is in geostrophic balance. If along-slope pressure gradients are weak or integrate to zero in the case of a circumpolar flow, then a mean cross-slope flow \bar{v} cannot be supported. In this case, the mean overturning is similar to the ACC's Deacon cell⁷: vertical velocities connect Ekman layers at the surface and sea floor. However, in the absence of large vertical velocities, the overturning may be closed in the interior by an eddy transport, directed along density surfaces and mediated by correlations in cross-slope velocity and density layer thickness anomalies $\overline{v'h'}$. At the shelf break, both ψ_w and ψ_e act to release available potential energy, whereas buoyancy forcing on the shelf is a source of available potential energy that maintains the tilted isopycnals.

Direct resolution of these dynamics in numerical models requires 1 km grid spacing²⁴, for $\lambda \approx 5 \text{ km}$. Application of the Gent–McWilliams diffusive parameterization²⁵ encourages the relaxation of tilted density surfaces towards a horizontal orientation. However, the extraction of potential energy from the background stratification is minimized not when the density surfaces are flat, but rather when they are parallel to the bottom slope²⁶. A PV-based parameterization may provide a more accurate representation of the eddy fluxes in this case.

Characteristics of the northwestern Weddell Sea circulation will be similar to a large fraction of the Antarctic margins, because surface winds are the primary mechanical forcing and the shelf break is dominated by westward slope currents²³. Bathymetric features, such as troughs and ridges, may locally enhance eddy generation and thus lead to circum-Antarctic variability in values of K . However, in an along-stream-averaged sense, eddies are still required to close the overturning²⁴. The identification of an eddy overturning departs from models of cross-shelf transport involving friction or along-stream pressure gradients^{16,27}. Lateral stirring by an active eddy field may vary in response to long-term changes in surface wind and buoyancy forcing and contribute to observed changes in AABW properties²⁸. This study focuses on mass transport, but eddy stirring also influences property fluxes. Onshore heat fluxes will be particularly sensitive to the eddy component because heat content is dominated by layers away from surface and bottom boundaries. Understanding the spatial distribution of mesoscale variability and its influence on the delivery of heat onto the continental shelf is needed to reduce uncertainty in rates of ice sheet retreat²⁹.

Methods

Three ocean gliders were deployed from the RRS *James Clark Ross* in the Weddell Sea between 20 January and 13 March 2012 (Fig. 1) as part of the GENTOO (Gliders, Excellent New Tools for Observing the Ocean) project. In total the gliders completed over 750 dives, to a depth of 1,000 m or to within 20 m of the bottom in shallower water. The gliders collected vertical profiles of temperature and salinity, dissolved oxygen, optical backscatter and fluorescence. Here we focus on the hydrographic data. Temperature and salinity data were collected using a Sea-Bird Electronics CT Sail; temperature and salinity were converted into neutral density surfaces. Glider station spacing varied between two and five kilometres on the basis of current speed and water column depth. This spacing improves on traditional ship-based surveys by roughly an order of magnitude.

The gliders complete a V-shaped dive approximately every four hours (depending on water column depth), making measurements every 5 s, or approximately every 0.5 m. The PV sections shown in this study are based on optimally interpolated sections with a vertical resolution of 5 m and a horizontal resolution of 2 km. The geostrophic shear is obtained by first filtering the data using a boxcar filter that extends 4 km in the horizontal and 10 m in the vertical, for example, three grid points in each direction. The velocity and density structure of the sections were found to be insensitive to this smoothing, as long as the filter did not exceed 10 km in the horizontal and 30 m in the vertical. The barotropic, or depth-averaged component of the velocity, is calculated directly from the gliders using both the glider surfacing positions and a glider flight model. These are shown to produce good agreement with surface drifter velocities obtained during the same cruise³⁰.

The Ertel PV is defined by

$$Q_{\text{full}} = (f\hat{\mathbf{k}} + \nabla \times \mathbf{u}) \cdot \nabla b \quad (3)$$

where $\nabla \times \mathbf{u}$ and b are relative vorticity and buoyancy. Buoyancy is defined by $b = -g\rho_0^{-1}(\rho - \rho_0)$, where the density ρ refers to neutral density and ρ_0 is a reference value. Along a single section, Q_{full} must be approximated because only the cross-section (in this case, along-slope) component of the velocity is measured. PV calculated from the available, observed quantities leads to $Q = fb_z + u_z b_y - u_y b_z$, where subscripts represent partial derivatives; z increases upward and y increases shoreward. In the limit that the Rossby number is small, $Q \approx fb_z$, that is, the stretching component of the PV is dominant. From observations, we find that along the flanks of the strongest shelf-break jets, the lateral shear can be sufficiently large to make a non-negligible contribution to Q . However, over most of the domain the assumption that Q is controlled by density layer fluctuations is valid. The emphasis of the analysis is on the statistical properties of the PV field across multiple sections.

For the analysis carried out using equations (1) and (2), we use data from the glider sections to obtain the following values: $M^2 = b_z = 1.3 \times 10^{-8} \text{ s}^{-2}$, $N^2 = b_z = 2 \times 10^{-6} \text{ s}^{-2}$, $\ell = 10 \text{ km}$, $\rho_0 = 1,027.8 \text{ kg m}^{-3}$, $f = -1.3 \times 10^{-4}$, $\tau = -0.04 \text{ N m}^{-2}$, $\partial_y \bar{u}_{\text{CDW}} = 0.01$. The along-slope wind stress is assumed negative if the coast is to the left of the wind direction; this corresponds to easterlies over much of the Antarctic margins. We take the width of the baroclinic zone to be the horizontal length scale associated with the jet spacing over the slope. As stated in the manuscript, this length scale agrees with the Rhines scale.

To calculate the deformation radius λ , H takes values between 500 and 1,000 m over our glider sections.

All data used in this study are archived at the British Oceanographic Data Centre, www.bodc.ac.uk, cruise JR255A.

Received 23 April 2014; accepted 9 October 2014;
published online 10 November 2014

References

- Gill, A. E. Circulation and bottom water production in the Weddell Sea. *Deep Sea Res.* **20**, 11–140 (1973).
- Shepherd, A., Wingham, D. & Rignot, E. Warm ocean is eroding West Antarctic ice sheet. *Geophys. Res. Lett.* **31**, L23402 (2004).
- Pritchard, H. D. *et al.* Antarctic ice-sheet loss driven by basal melting of ice shelves. *Nature* **484**, 502–505 (2012).
- Rignot, E., Jacobs, S., Mouginot, J. & Scheuchl, B. Ice-shelf melting around Antarctica. *Science* **341**, 266–270 (2013).
- Thoma, M., Jenkins, A., Holland, D. & Jacobs, S. Modelling circumpolar deep water intrusions on the Amundsen Sea continental shelf, Antarctica. *Geophys. Res. Lett.* **35**, L18602 (2008).
- Schodlok, M. P., Menemenlis, D., Rignot, E. & Studinger, M. Sensitivity of the ice-shelf/ocean system to the sub-ice-shelf cavity shape measured by NASA Icebridge in Pine Island Glacier, West Antarctica. *Ann. Glaciol.* **53**, 156–162 (2012).
- Marshall, J. & Speer, K. Closure of the meridional overturning circulation through Southern Ocean upwelling. *Nature Geosci.* **5**, 171–180 (2012).
- Dinniman, M. S., Klinck, J. M. & Smith, W. O. Jr A model study of circumpolar deep water on the West Antarctic Peninsula and Ross Sea continental shelves. *Deep Sea Res. II* **58**, 1508–1523 (2011).
- Nøst, O. A. *et al.* Eddy overturning of the Antarctic slope front controls glacial melting in the eastern Weddell Sea. *J. Geophys. Res.* **116**, C11014 (2011).
- Stewart, A. L. & Thompson, A. F. Connecting Antarctic cross-slope exchange with Southern Ocean overturning. *J. Phys. Oceanogr.* **43**, 1453–1471 (2013).
- Gordon, A. L., Huber, B., McKee, D. & Visbeck, M. A seasonal cycle in the export of bottom water from the Weddell Sea. *Nature Geosci.* **3**, 551–556 (2010).
- Spall, M. A. Dense water formation around islands. *J. Geophys. Res.* **118**, 2507–2519 (2013).
- Orsi, A. H., Johnson, G. C. & Bullister, J. L. Circulation, mixing, and production of Antarctic Bottom Water. *Prog. Oceanogr.* **43**, 55–109 (1999).
- Korb, R. E. & Whitehouse, M. Contrasting primary production regimes around South Georgia, Southern Ocean: Large blooms versus high nutrient, low chlorophyll waters. *Deep Sea Res. I* **51**, 721–738 (2004).
- Tagliabue, A., Bopp, L. & Aumont, O. Evaluating the importance of atmospheric and sedimentary iron sources to Southern Ocean biogeochemistry. *Geophys. Res. Lett.* **36**, L13601 (2009).
- Baines, P. G. & Condie, S. *Ocean, Ice and Atmosphere: Interactions at the Antarctic Continental Margins, Antarctic Research Series Vol. 75*, 29–49 (1998).
- Speer, K., Rintoul, S. R. & Sloyan, B. The diabatic Deacon cell. *J. Phys. Oceanogr.* **30**, 3212–3222 (2000).
- Jullion, L. *et al.* Decadal freshening of the Antarctic bottom water exported from the Weddell Sea. *J. Clim.* **26**, 8111–8125 (2013).
- Jacobs, S. S. On the nature and significance of the Antarctic slope front. *Mar. Chem.* **35**, 9–24 (1991).
- Plumb, R. A. Three-dimensional propagation of transient quasi-geostrophic eddies and its relationship with the eddy forcing of the time-mean flow. *J. Atmos. Sci.* **43**, 1657–1678 (1986).
- Spall, M. A., Pickart, R. S., Fratantoni, P. S. & Plueddemann, A. J. Western Arctic shelfbreak eddies: Formation and transport. *J. Phys. Oceanogr.* **38**, 1644–1668 (2008).
- Visbeck, M., Marshall, M., Haine, T. & Spall, M. Specification of eddy transfer coefficients in coarse-resolution ocean circulation models. *J. Phys. Oceanogr.* **27**, 381–402 (1997).
- Wählin, A. K., Yuan, X., Björk, G. & Nohr, C. Inflow of warm Circumpolar Deep Water in the central Amundsen shelf. *J. Phys. Oceanogr.* **40**, 1427–1434 (2010).
- St Laurent, P., Klinck, J. M. & Dinniman, M. S. On the role of coastal troughs in the circulation of warm circumpolar deep water on Antarctic shelves. *J. Phys. Oceanogr.* **43**, 51–64 (2013).
- Gent, P. R. & McWilliams, J. C. Isopycnal mixing in ocean circulation models. *J. Phys. Oceanogr.* **20**, 150–155 (1990).
- Isachsen, P. E. Baroclinic instability and eddy tracer transport across sloping bottom topography: How well does a modified Eady model do in primitive equation simulations? *Ocean Model.* **39**, 183–199 (2011).

27. Ou, H.-W. Watermass properties of the Antarctic slope front: A simple model. *J. Phys. Oceanogr.* **37**, 50–59 (2007).
28. Purkey, S. G. & Johnson, G. C. Global contraction of Antarctic bottom water between the 1980s and 2000s. *J. Clim.* **25**, 5830–5844 (2012).
29. Joughin, I., Smith, B. E. & Medley, B. Marine ice sheet collapse potentially under way of the Thwaites glacier basin, West Antarctica. *Science* **344**, 735–738 (2014).
30. Thompson, A. F. & Youngs, M. K. Surface exchange between the Weddell and Scotia Seas. *Geophys. Res. Lett.* **40**, 5920–5925 (2013).

Acknowledgements

The authors thank the officers and crew of the RRS *James Clark Ross* for help in deploying and recovering the gliders. A.F.T. was financially supported by NSF award OPP-1246460. S.S. and K.J.H. were financially supported by the NERC Antarctic Funding Initiative

research grant GENTOO NE/H01439X/1. A.L.S. was supported by the President's and Director's Fund program at Caltech.

Author contributions

K.J.H. and A.F.T. conceived and designed the field program; A.F.T., K.J.H. and S.S. collected the data; S.S. processed the data; A.F.T. and S.S. analysed the data; A.F.T., K.J.H., S.S. and A.L.S. co-wrote the paper.

Additional information

Supplementary information is available in the [online version of the paper](#). Reprints and permissions information is available online at www.nature.com/reprints. Correspondence and requests for materials should be addressed to A.F.T.

Competing financial interests

The authors declare no competing financial interests.